Supporting Information

Fe_3O_4/FeS_2 Heterostructures Enable Efficient Oxygen Evolution Reaction

*Min Jie Wang, [a, b] Xingqun Zheng, [a] Lele Song, [a] Xin Feng, [c] Qiang, Liao, [d, e] Jing Li, *, [a, d] Li Li, *, [a] and Zidong Wei, *, [a]*

[a]School of Chemistry and Chemical Engineering, Chongqing University, Shazhengjie 174, Chongqing 400044, China.
[b]School of Chemistry and Environmental Engineering, Shenzhen University, Shenzhen, Guangdong, 518060, P.R. China.
[c]School of Materials Science and Engineering, Chongqing University, Shazhengjie 174, Chongqing 400044, China.
[d]National-municipal Joint Engineering Laboratory for Chemical Process Intensification and Reaction, Chongqing University, Shazhengjie 174, Chongqing 400044, China.
[e]Key Laboratory of Low-grade Energy Utilization Technologies and Systems, Ministry of Education, Institute of Engineering Thermophysics, School of Energy and Power Engineering, Chongqing University, Shazhengjie 174, Chongqing 400044, China.

E-mail: lijing@cqu.edu.cn; liliracial@cqu.edu.cn; zdwei@cqu.edu.cn.

Experimental Sections

Synthesis of Fe_3O_4 microspheres

Fe_3O_4 microspheres were prepared according to the reported method.[1] In a typical process, $FeCl_3 \cdot 6H_2O$ and NaAc were dissolved in 60 mL of ethylene glycol to form a solution containing 7.49 mM Fe^{3+} and 65.85 mM Ac^-. This solution was sealed in a Teflon-lined autoclave with a volume of 100 mL to conduct a hydrothermal reaction at 200 °C for 8 hours. The obtained Fe_3O_4 powder was washed several times with ethanol and dried under vacuum at 60 °C.

Preparation of Fe_3O_4/FeS_2-*x*

The Fe_3O_4 was further sulfurized to get the Fe_3O_4/FeS_2-*x* products. Two porcelain boats were placed in a quartz tube with one located in the middle position filled with Fe_3O_4 powder, and the other one placed near the gas inlet added with thiourea. The furnace was heated to 350 °C at a heating rate of 2.0 °C min^{-1} and then maintained at the same temperature for 2 h under continuous N_2 purge to get the final products. Particularly, the mass of Fe_3O_4 added in the reaction was fixed at 200 mg, and the amount of thiourea was changed from 200 mg, to 500 mg, 1000 mg, and 2000 mg, by which the Fe_3O_4/FeS_2-*x* products (where *x* represents the mass ratio of thiourea to Fe_3O_4) with verified sulfurization degrees, $Fe_3O_4Fe_3O_4/FeS_2$-1, Fe_3O_4/FeS_2-2.5, Fe_3O_4/FeS_2-5, and Fe_3O_4/FeS_2-10 (also named FeS_2) can be achieved.

Characterizations

Field emission scanning electron microscopy (FESEM) measurements were conducted on a JEOL JSM-7800F microscope operated at 10 kV. Transmission electron microscopy (TEM) images were collected on a FEI Tecnai G2 T20 microscope, and scanning transmission electron microscopy (STEM) measurements were conducted on a FEI Tecnai G2 F20 FEGTE

microscope operated at an accelerating voltage of 200 kV. X-ray photoelectron spectra (XPS) were recorded on a Thermal ESCALAB 250 XI. X-ray diffraction (XRD) data were collected on a Shimadzu X-ray diffractometer, model 6000 at a scanning rate of 10° min^{-1}.

Electrochemical measurements

The catalyst ink was prepared by adding 5.0 mg of Fe_3O_4-FeS_2-*x* catalyst powder and 40 μL of 5.0 wt% nafion solution into 0.5 mL of ethanol under ultrasonation.[2] This uniform dispersion was then loaded onto a piece of clean Ni foam and dried under vacuum at 30 °C. Typically, the loading of Fe_3O_4-FeS_2-*x* is 1.0 mg cm^{-2}. And for commercial RuO_2/C which is used as the benchmark catalyst for comparison in this work, the loading is 1.0 mg_{Ru} cm^{-2}.[3]

The electrochemical performances were measured in a three-electrode system with our products as working electrodes, a graphite rod as the counter electrode, a Hg/HgO as the reference electrode, and O_2 purged 1.0 M KOH aqueous solution as the electrolyte.[3] The current density was normalized to the geometrical surface area and all reported potentials were given relative to the reversible hydrogen electrode (RHE). The linear sweep voltammogram (LSV) curves were collected in the range of 1.2-1.7 V at a scan rate of 5 mV s^{-1}, and the electrochemical impedance spectra (EIS) measurements were performed under potentiostatic state from 100 K - 0.01 Hz. All polarization curves were corrected by an *iR* compensation using the equation (1), except chronoamperometric response (*i*-*t*) curves,

$$E_{\text{corrected}} = E_{\text{uncorrected}} - iRs, \qquad (1)$$

in which *i* and *Rs* represent the current density and solution impedance, respectively. The electrochemical durability was evaluated by scanning 2000 continuous cycles of the cyclic voltammetry curves, and recording *i*-*t* curves at 10 mA cm^{-2} for uninterrupted 36 hours.

Theoretical Calculations

In this work, periodic density functional theory (DFT) calculations were conducted by using the Vienna Ab-initio Simulation Program (VASP).[4] The ionic cores were described by the projector augmented wave (PAW) method.[5] And the electron exchange-correlation was modeled by virtue of the Perdew-Burke- Ernzerhof (PBE) function within generalized gradient approximation (GGA).[6] A cutoff energy of 450 eV was carried out to the plane-wave basis set. The convergence criterion was 10^{-5} eV for energy and 0.01 eV/Å for force. (the DFT-D3 method was used to calculate the explicit dispersion correction and solvent effect terms to the energy[7, 8], and VASPsol.[9] , respectively). The Monkhorst−Pack k-point mesh was set to be 3 × 1 × 1 for all systems. To separate adjacent periodic images a 10 Å thick vacuum along the vertical direction was added. The FeS_2 surface was simulated by cleaving the (1x1) FeS_2 (210) surface from FeS_2 bulk cell. To simulate the interface (or the partial oxidation) of FeS_2 surface, the O modified FeS_2 (210) surface was created by substituting one of the top surface S atoms with an O atom.

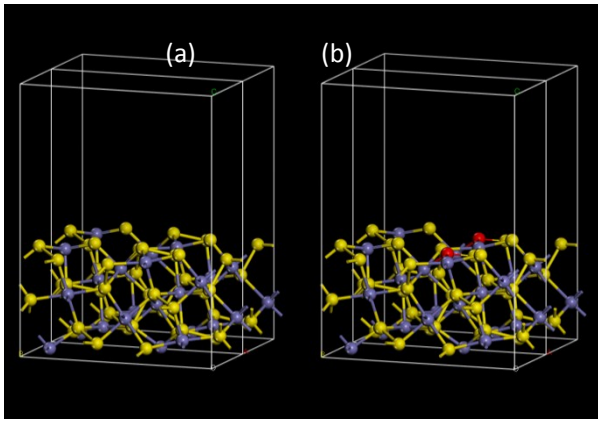

The three-dimension structure of periodic (a) FeS_2 (210) and (b) O-FeS_2(210) slabs.

The key OER steps include:

$$H_2O + * \rightarrow *OH + H^+ + e^- \quad (1)$$

$$*OH \rightarrow O* + H^+ + e^- \quad (2)$$

$$O* + H_2O \rightarrow *OOH + H^+ + e^- \quad (3)$$

$$*OOH \rightarrow * + O_2 + H^+ + e^- \quad (4)$$

The adsorption free energy of intermediates were calculated using the equations:

$$\Delta G_{*OH} = G_{*OH} + \frac{1}{2}G_{H_2} - G_* - G_{*H_2O} - (eU)$$

$$\Delta G_{*O} = G_{*O} + G_{H_2} - G_* - G_{*H_2O} - (2eU)$$

$$\Delta G_{*OOH} = G_{*OOH} + \frac{3}{2}G_{H_2} - G_* - 2G_{*H_2O} - (3eU)$$

$$\Delta G_{*O_2} = G_{*O_2} + 2G_{H_2} - G_* - 2G_{*H_2O} - (4eU)$$

The Gibbs free energy G was calculated as follow:

$$G = E + ZPE - TS$$

where *G*, *E*, *ZPE* and *TS* are the free energy, total energy from DFT calculations, zero point energy and entropic contributions (T was set to be 300K), respectively. *ZPE* could be derived after frequency calculation by:

$$ZPE = \frac{1}{2}\sum hv_i$$

And the *TS* is entropic contribution values of adsorbed species (T was set to be 300K) which are calculated after obtaining the vibrational frequencies

$$TS = k_B T[\sum \ln\left(\frac{1}{1 - e^{-hv_i/k_B T}}\right) + \sum \frac{hv}{k_B T}\frac{1}{(e^{hv_i/k_B T} - 1)} + 1]$$

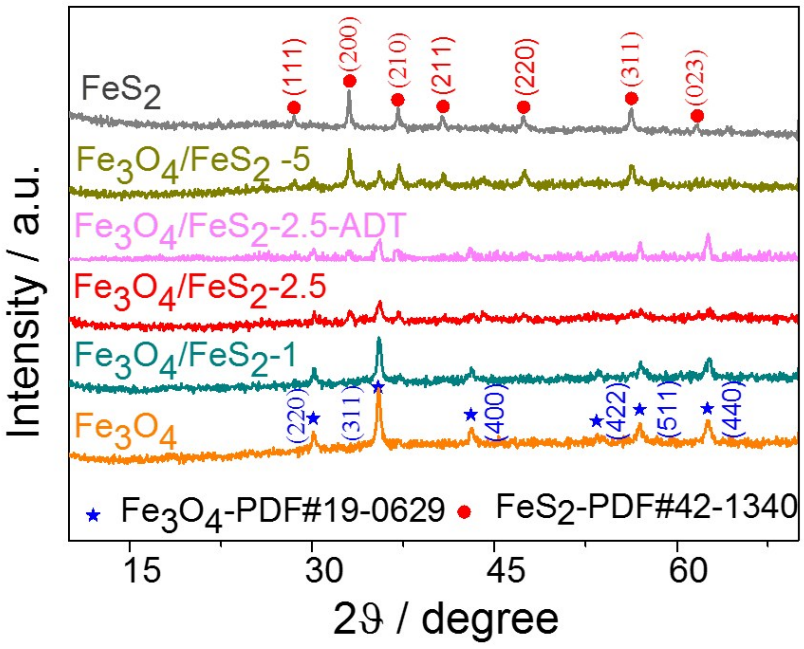

Figure S1. The X-ray diffraction (XRD) patterns.

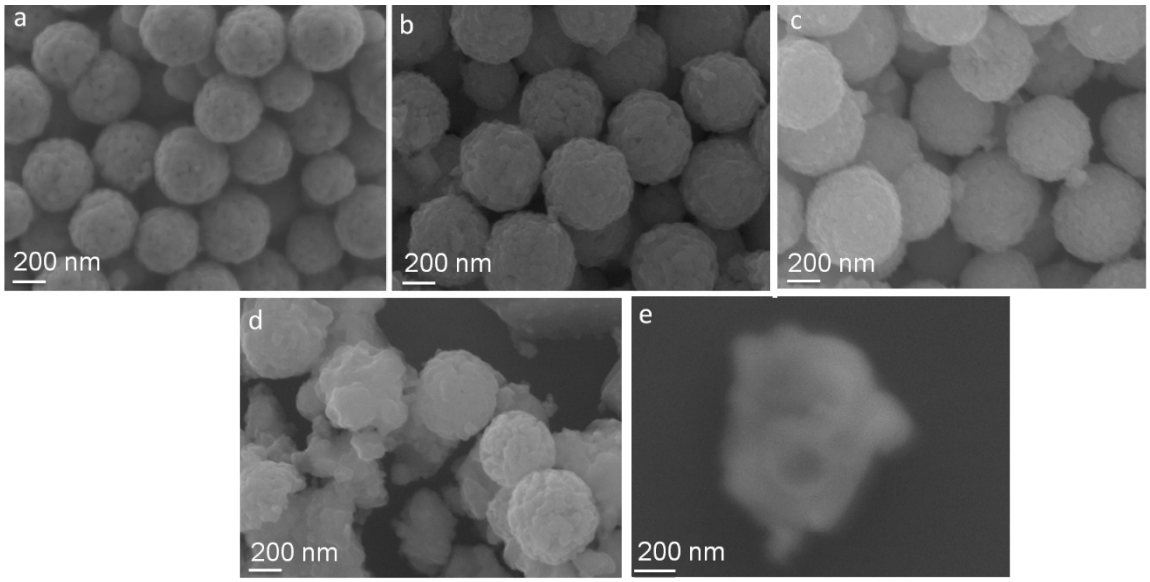

Figure S2. The SEM and TEM images of Fe_3O_4 (a), Fe_3O_4/FeS_2-1 (b); Fe_3O_4/FeS_2-2.5 (c); Fe_3O_4/FeS_2-5 (d); FeS_2 (Fe_3O_4/FeS_2-10) (e).

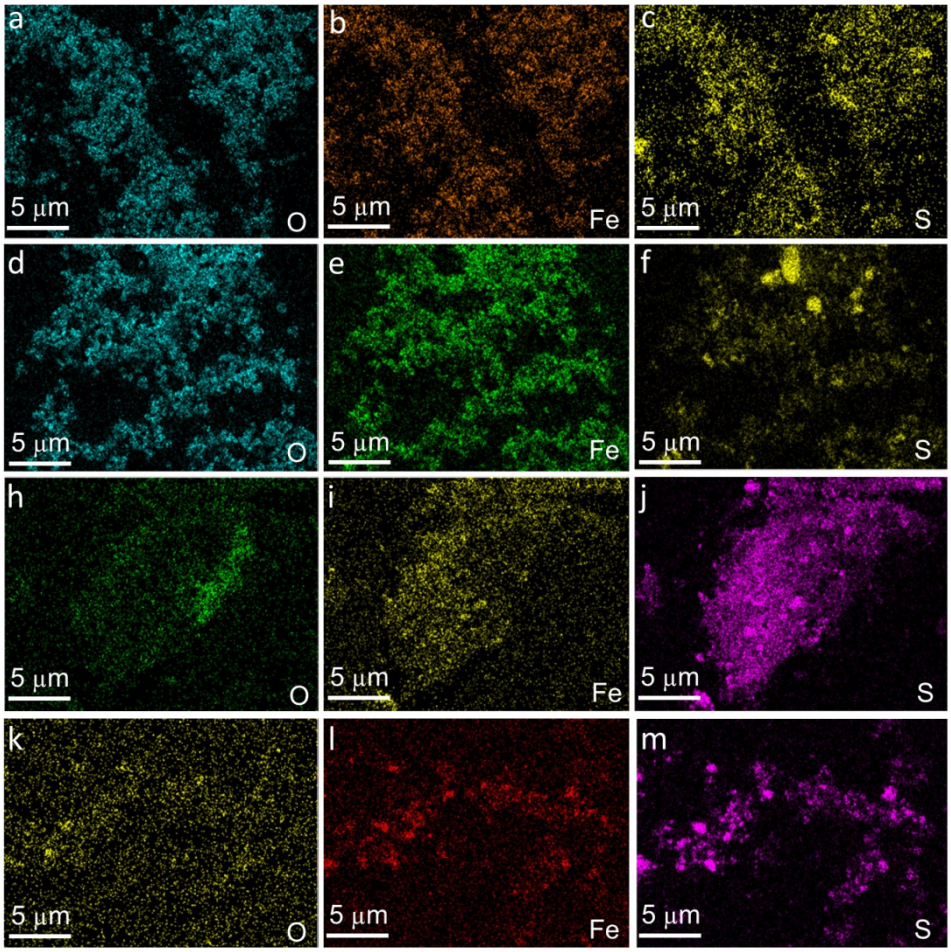

Contents (at. %) / Samples	O	Fe	S
Fe_3O_4/FeS_2-1	53.3	39.7	7.0
Fe_3O_4/FeS_2-2.5	48.6	40.0	11.4
Fe_3O_4/FeS_2-5	31.2	38.2	38.2
Fe_3O_4/FeS_2-10	18.5	30.7	50.8

Figure S3. The EDS mappings of elemental O, Fe, and S, and the detected atomic contents. (a - c) Fe_3O_4/FeS_2-1; (d - f) Fe_3O_4/FeS_2-2.5; (h - j) Fe_3O_4/FeS_2-5; (k - m) FeS_2 (Fe_3O_4/FeS_2-10).

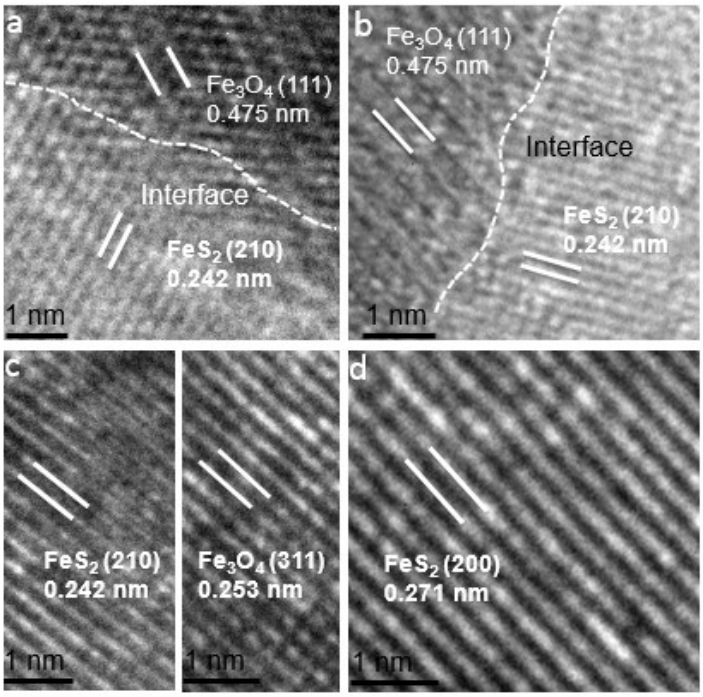

Figure S4. The HRTEM images for the sample Fe_3O_4/FeS_2-1 (a), Fe_3O_4/FeS_2-2.5 (b), Fe_3O_4/FeS_2-5 (c), and FeS_2 (d).

Table S1. Comparison of the electrocatalytic OER performances of our catalysts with literature results. The electrolyte is 1.0 M KOH solution.

Electrocatalyst	Current density (mA cm^{-2})	Overpotential η (mV)	Tafel slop (mV dec^{-1})	Reference
Fe_3O_4-FeS_2-2.5	10	253	48	**This work**
NiCoFe-MOF	10	257	41	[10]
rGo@$CoFe_2O_4$	10	300	36	[11]
FeNi/$NiFe_2O_4$@NC	10	316	60	[12]
NC-MUV-$3_{Fe\text{-}ZIF8}$	10	316	37	[13]
$Co_{0.15}Fe_{0.85}N_{0.5}$NSs	10	266	30	[14]
(Ni, Fe)S_2@MoS_2	10	270	43	[15]
FN-2 $_{Fe+Ni\text{-}MOFs}$	10	275	57	[16]
$NiFe_2O_{4(QDs)}$/CNTs	10	450	50	[17]
Fe_4P	10	283	41	[18]
CoFe LDHs-Ar	10	266	38	[19]
S-Fe_3O_4/NF	10	279	118	[20]

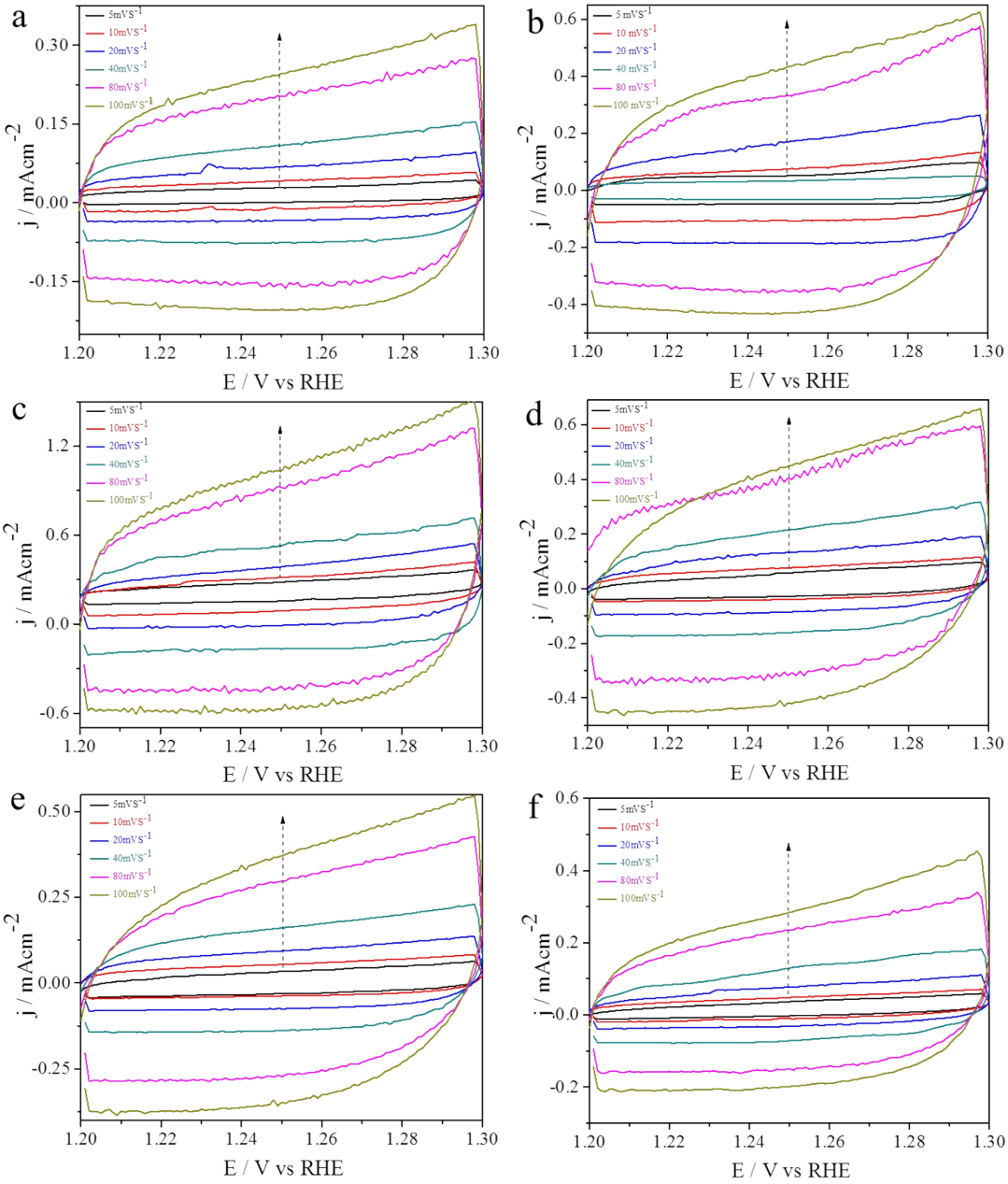

Figure S5. CV curves of the samples against scanning rates from 5 mV s^{-1} to 100 mV s^{-1}. (a) Fe_3O_4; (b) Fe_3O_4/FeS_2-1; (c) Fe_3O_4/FeS_2-2.5; (d) Fe_3O4/FeS_2-5; (e) Fe_3O_4/FeS_2-10; (f) Fe_3O_4+FeS_2.

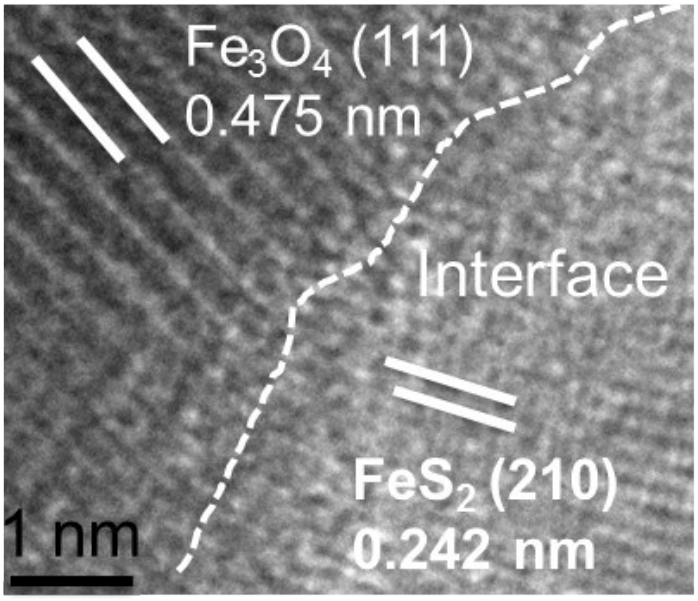

Figure S6. The HRTEM image of Fe_3O_4/FeS_2-2.5-ADT.

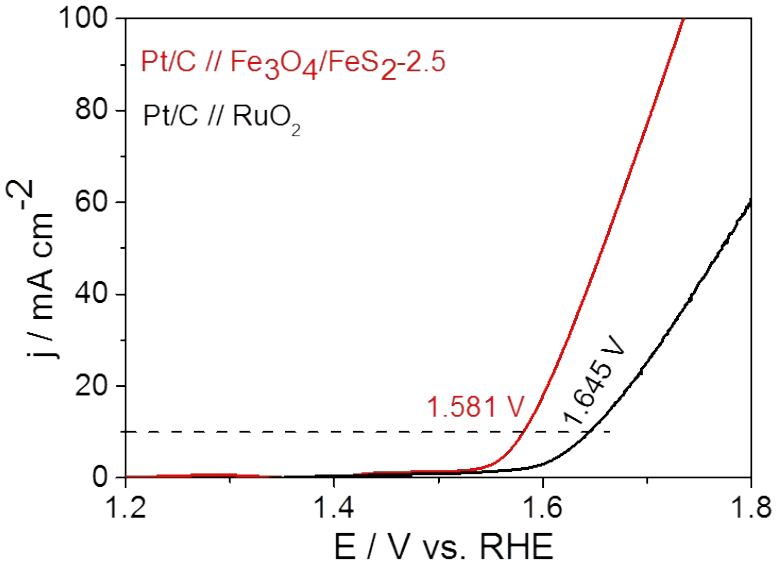

Figure S7 Polarization curves of water splitting measured in 1.0 M KOH.

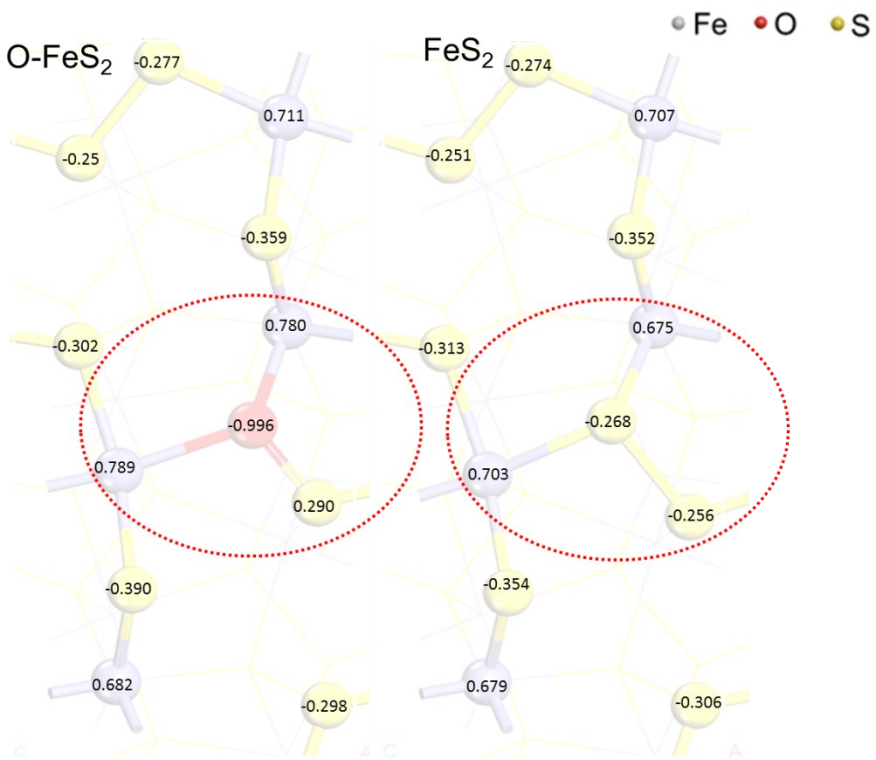

Figure S8. Bader charge of O-FeS_2 and FeS_2

References

[1] J. Liu, Z. Sun, Y. Deng, Y. Zou, C. Li, X. Guo, L. Xiong, Y. Gao, F. Li, D. Zhao, *Angew. Chem. Int. Ed.* 2009, **48**, 5875-5879.

[2] Y. P. Zhu, T. Y. Ma, M. Jaroniec, S. Z. Qiao, *Angew. Chem. Int. Ed.* 2017, **56**, 1324-1328.

[3] L. Peng, J. Wang, Y. Nie, K. Xiong, Y. Wang, L. Zhang, K. Chen, W. Ding, L. Li, Z. Wei, *ACS Catal.* 2017, **7**, 8184-8191.

[4] G. Kresse, J. Furthmüller , *Phys.Rev. B* 1996**, 54**, 11169.

[5] P. Rochana, E. Ozdogan, K. Lee, J. Wilcox, *Energy Procedia* 2013, **37**, 1093-1103.

[6] J. P. Perdew, K. Burke, M. Ernzerhof, *Phys.rev. lett.* 1996, **77**, 3865.

[7] S. Bureekaew, R. Schmid, *Crystengcomm* 2013, **15**, 1551-1562.

[8] G. Stefan, E. Stephan, G. Lars, *J. Comput. Chem.* 2011, **32**, 1456-1465.

[9] K. Mathew, R. Sundararaman, K. Letchworthweaver, T. A. Arias, R. G. Hennig, *J. Chem. Phys.* 2014, **140**, 084106.

[10] Q. Qian, Y. Li, Y. Liu, L. Yu, G. Zhang, *Adv. Mater.* 2019*,* **31***,* 1901139.

[11] J. Li, Q. Zhou, C. Zhong, S. Li, Z. Shen, J. Pu, J. Liu, Y. Zhou, H. Zhang, and H. Ma, *ACS Catal.* 2019, **9**, 3878-3887.

[12] Z. Zou, T. Wang, X. Zhao, W. Jiang, H. D. Gao, *ACS Catal.* 2019, **9**, 7356-7364.

[13] J. López-Cabrelles, J. Romero, G. Abellán, M. G. M. Palomino, S. Valencia, F. Rey, and G. M. Espallargas, *J. Am. Chem. Soc.* **2019**, *141*, 7173.

[14] L. An, J. Feng, Y. Zhang, Y. Zhao, R. Si, G. Wang, F. Cheng, P. Xi, S. Sun, *Nano Energy* 2019, **57**, 644-652.

[15] Y.Liu, S. Jiang, S. Li, L. Zhou, Z. Li, J. Li, M. Shao, *Appl. Catal. B: Environ.* 2019, **247**, 107-114.

[16] M. Liu, L. Kong, X. Wang, J. He, and X. Bu, *Small* 2019, 1903410.

[17] N. Xu, Y. Zhang, T. Zhang, Y. Liu, J. Qiao, *Nano Energy* 2019, **57**, 176-185.

[18] Q. He, H. Xie, Z. Rehman, C. Wang, P. Wan, H. Jiang, W. Chu, and L. Song, *ACS Energy Lett.* 2018, **3**, 861-868.

[19] Y. Wang, Y. Zhang, Z. Liu, C. Xie, S. Feng, D. Liu, M. Shao, S. Wang, *Angew. Chem. Int. Ed.* 2017, **56**, 5867-5871.

[20] J. Liu, D. Zhu, T. Ling, A. Vasileff, S.-Z. Qiao, *Nano Energy* 2017, **40**, 264-273.